Advances in Water Resources

# Non-Darcian flow of shear-thinning fluids through packed beads: Experiments and predictions using Forchheimer's law and Ergun's equation

Antonio Rodríguez de Castro[a,b,*], Giovanni Radilla[a,c]

[a] Arts et Métiers ParisTech, Rue Saint-Dominique, 51006 Châlons-en-Champagne, France
[b] MSMP – EA7350, Rue Saint Dominique, 51006 Châlons-en-Champagne, France
[c] LEMTA, UMR 7563, CNRS, 54518 Vandœuvre-lès-Nancy, France

A B S T R A C T

The flow of shear-thinning fluids through unconsolidated porous media is present in a number of important industrial applications such as soil depollution, Enhanced Oil Recovery or filtration of polymeric liquids. Therefore, predicting the pressure drop–flow rate relationship in model porous media has been the scope of major research efforts during the last decades. Although the flow of Newtonian fluids through packs of spherical particles is well understood in most cases, much less is known regarding the flow of shear-thinning fluids as high molecular weight polymer aqueous solutions. In particular, the experimental data for the non-Darcian flow of shear-thinning fluids are scarce and so are the current approaches for their prediction. Given the relevance of non-Darcian shear-thinning flow, the scope of this work is to perform an experimental study to systematically evaluate the effects of fluid shear rheology on the flow rate–pressure drop relationships for the non-Darcian flow through different packs of glass spheres. To do so, xanthan gum aqueous solutions with different polymer concentrations are injected through four packs of glass spheres with uniform size under Darcian and inertial flow regimes. A total of 1560 experimental data are then compared with predictions coming from different methods based on the extension of widely used Ergun's equation and Forchheimer's law to the case of shear thinning fluids, determining the accuracy of these predictions. The use of a proper definition for Reynolds number and a realistic model to represent the rheology of the injected fluids results in the porous media are shown to be key aspects to successfully predict pressure drop–flow rate relationships for the inertial shear-thinning flow in packed beads.

## 1. Introduction

Diverse industrial applications involve the flow of shear-thinning fluids in porous media, including soil remediation, filtration of polymeric liquids and slurries, oil recovery and $CO_2$ underground storage (Fourar et al., 2004; Fayed et al., 2016). In particular, shear-thinning fluids are commonly injected in Enhanced Oil Recovery (EOR) to reduce the amount of unrecovered oil after waterflooding by reducing mobility in high-permeability layers and creating a transverse pressure gradient that promotes fluid migration into less permeable layers (Silva et al., 2012). Most of the heavy oil reservoirs belong to unconsolidated formations (Pang and Liu, 2013). Therefore, predicting the relationships between flow rate and pressure drop for shear-thinning fluids flow in unconsolidated porous media is of vital importance and has been the scope of major research efforts (Chhabra and Srinivas, 1991; Rao and Chhabra, 1993; Smit and du Plessis, 1997; Tiu et al., 1997; Machac et al., 1998; Chhabra et al., 2001). The flow of shear-thinning fluids through beds of spherical particles represents an idealization of many industrially important processes as those mentioned before (Tiu et al., 1997). For this reason, most of the experimental works have been conducted with beds of spherical particles (Rao and Chhabra, 1993; Tiu et al., 1997; Machac et al., 1998).

The objective of this work is to experimentally assess the efficiency of the commonly used Forchheimer's law and Ergun's equation to predict pressure drop–flow rate relationship for non-Darcian flow regime in the case of shear-thinning fluids injected through model unconsolidated porous media. In order to achieve this goal, xanthan gum biopolymer aqueous solutions were injected through different packs of spherical glass beads covering

* Corresponding author at: Arts et Métiers ParisTech, Rue Saint-Dominique, 51006 Châlons-en-Champagne, France.
*E-mail address:* antonio.rodriguezdecastro@ensam.eu (A. Rodríguez de Castro).

Darcian and non-Darcian flow regimes. The effect of polymer concentration and the beads size on the importance of inertial effects and the accuracy of these predictions is evaluated and discussed.

It should be noted that elongational flows during the injection of solutions of polymers presenting a certain degree of flexibility through porous media are known to induce extra pressure losses with respect to pure shear flow (Rodríguez et al., 1993; Müller and Sáez, 1999; Nguyen and Kausch, 1999; Seright et al., 2011; Amundarain et al., 2009). These extra pressure losses were attributed to the formation of transient entanglements of polymer molecules due to the action of the extensional component of the flow. In the present work, we first hypothesize that the deviation of the experimentally measured pressure drop with respect to the linear pressure drop predicted from the shear viscosity of the fluid can be explained in terms of inertial effects generated in the porous medium flow. This hypothesis is then validated through analysis of the experimental results.

## 2. Background

Single-phase flow of incompressible Newtonian fluids through porous media is governed by Darcy's law (Darcy, 1856). Nevertheless, this law is only valid when inertial forces are negligible compared to viscous forces (Schneebeli, 1955; Hubbert, 1956; Scheidegger, 1960; Chauveteau and Thirriot, 1967). This is not the case of many situations where the inertial effects are important, e.g. prediction of well performance (Zen and Grigg, 2006) and flow through fractured media (Radilla et al., 2013). In the post-Darcy regime, two equations are invariably used to describe pressure drop as a function of flow rate (Dukhan et al., 2014): Forcheimer's equation (Forchheimer, 1901) and Ergun's equation (Ergun, 1952). Forchheimer's empirical law is commonly used to model the strong inertial regime through addition of a quadratic flow rate term to Darcy's law to describe the deviations from linearity and. This law has been experimentally validated (Dullien and Azzam, 1973; Geertsma, 1974; MacDonald et al., 1979; Rasoloarijaona and Auriault, 1994) and has found some theoretical justifications (Cvetkovic, 1986; Giorgi, 1997; Chen et al., 2001). This law is often expressed in terms of the form-and-inertia drag coefficient $F$, also known as the Forchheimer coefficient (Dukhan et al., 2014):

$$\nabla P = \frac{\Delta P}{L} = \frac{\mu}{K}u + \frac{\rho F}{\sqrt{K}}u^2 = \frac{\mu}{K}u + \rho\beta u^2 \tag{1}$$

where $\nabla P = \frac{\Delta P}{L}$ is the pressure gradient, $\Delta P$ is the absolute value of the pressure drop over a distance $L$, $\mu$ the viscosity of the injected fluid, $K$ is the intrinsic permeability, $\rho$ is the fluid density, $\beta$ is the inertial coefficient, $u = Q/S$ is the average velocity, $Q$ is the volumetric flow rate and $S$ is the cross-sectional area.

$F$ depends on the internal structure of the porous medium and was reported to be universal for a given class of porous media (Hwang et al., 2002; Liu et al., 2006; Dukhan and Patel, 2011), which is not in agreement with the experimental results of some researchers (Beavers et al., 1973; Antohe et al., 1996; Lage and Antohe, 2000; Dukhan et al., 2014). Also, the ratio $\beta = \frac{F}{\sqrt{K}}$ depends on the structure and may contain information on tortuosity (Dukhan et al., 2014).

Fourar et al. (2004) performed numerical simulations to examine the viscous and pressure drags exerted by the solid grain on the fluid and their contribution to the deviation from Darcy's law in 2D and 3D porous media, identifying three laminar flow regimes: Darcy, transition and strong inertia. These authors found that the transition regime is narrower in the case of 3D porous media, which explains that the non-Darcy 3D-flow is correctly modeled by Forchheimer's equation in most cases without addition of a cubic deviation to represent the transition regime where cross viscous-inertia effects are significant (Fourar et al., 2004).

Ergun's equation is also widely used to link the relationship between pressure drop and flow rate to the structural characteristics of porous media (Ergun, 1952):

$$\frac{\Delta P}{L} = A\frac{(1-\varepsilon)^2\mu}{\varepsilon^3 d_s^2}u + B\frac{(1-\varepsilon)\rho}{\varepsilon^3 d_s}u^2 \tag{2}$$

where $\varepsilon$ is porosity, $d_s$ is the diameter of the packed particles, and $A$ and $B$ are empirical constants. In the case of spherical particles, the two most commonly used values for $A$ are 150 and 180 (Rao and Chhabra, 1993). $B = 1.75$ was originally proposed by Ergun (Ergun, 1952), but other values ranging from 1.8 to 4, depending on the roughness of the packed particles were subsequently reported (MacDonald et al., 1979). The construction of Ergun's equation was based on modeling the space between packed spheres as parallel capillaries, including multipliers to account for the geometrical differences (Klumpp et al., 2014; Dukhan et al., 2014). The range of applicability of this equation covers from creeping (Darcy) to turbulent flows. Both Forcheimer's law and Ergun equation are widely used to correlate pressure drop data. They both have a viscous linear term and a form/inertia quadratic term, but differ by multipliers. Dukhan et al. (2014) explored this difference and reconciled both equations in the case of Newtonian flow.

On the basis of the hydraulic radius theory, Kozeny–Carman equation provides the following relation between permeability and structural parameters in packed beds of spheres:

$$K = \frac{\varepsilon^3 d_s^2}{36\kappa(1-\varepsilon)^2} \tag{3}$$

where $\kappa$ is the Kozeny–Carman constant, which is commonly taken as identically 5 for spherical particles (Kaviany, 1995). $K$ can be predicted from $\varepsilon$ and $d_s$ using Eq. (3).

The relationships between $\Delta P$ and $Q$ data are often presented in a non-dimensional form involving two non-dimensional groups: friction factor $f$ and Reynolds number $Re$. The square root of the permeability determined in the Darcy regime was shown to be the most appropriate length scale for the definition of $Re$ and $f$ (Dybbs and Edwards, 1984; Kececioglu and Jiang, 1994; Boomsma and Poulikakos, 2002; Dukhan et al., 2014), giving the following expressions:

$$f = \frac{\Delta P}{L}\frac{\sqrt{K}}{\rho u^2} \tag{4}$$

$$Re = \frac{\rho u\sqrt{K}}{\mu} \tag{5}$$

Dybbs and Edwards (1984) obtained the following expression through correlation of experimental data for packed beads:

$$f = a\left(\frac{1}{Re}\right) + b \tag{6}$$

with $a$ and $b$ being constants. From Eqs. (2) and (3) the values of $a = A/(36\kappa)$ and $b = B/(6\varepsilon^{3/2}\sqrt{\kappa})$ are obtained, whereas the following expression is obtained from Forchheimer's law (Eq. (1)):

$$f = \left(\frac{1}{Re}\right) + F \tag{7}$$

The flow of Newtonian fluids through packed beads is well understood and allows process design calculations with acceptable levels of accuracy in most cases (Chhabra et al., 2001). However, much less is known about the flow of non-Newtonian fluids as high molecular weight polymer solutions. A review of non-Newtonian fluid flow and heat transfer in porous media was presented by Shenoy (1994), revealing that most concerned studies were restricted to Darcian flow. Also, Chhabra et al. (2001) reviewed the voluminous literature available on the flow of complex fluids through unconsolidated fixed and fluidized beds. Moreover, Sochi (2010) presented a review of continuum models, bundle of tubes models, numerical methods and pore-scale network

modeling in the context of single-phase flow of non-Newtonian fluids in porous media.

It can be deduced from the literature that considerable confusion exists regarding the definition of *Re* and f for the flow of shear-thinning fluids in porous media (Chhabra and Srinivas, 1991; Rao and Chhabra, 1993; Sabiri and Comiti, 1995; Tiu et al., 1997; Machac et al., 1998; Chhabra et al., 2001, Broniarz-Press et al., 2007; Amundarain et al., 2009, Fayed et al., 2016). In this respect, some researchers have highlighted the importance of using the actual shear viscosity of the fluid, which depends on the injection flow rate in the case of shear-thinning fluids, in the definition of *Re* (Chhabra et al., 2001; Broniarz-Press et al., 2007; Fayed et al., 2016).

Another significant challenge consisted in extending the existing macroscopic laws originally developed for Newtonian fluids to the case of non-Newtonian fluids flow. In this regard, Christopher and Middleman (1965) extended the Blake–Kozeny model to the flow of power-law fluids. Furthermore, Bird et al. (1987) used the single-capillary model to demonstrate that Darcy's law is also valid in the case of non-Newtonian fluids and Chhabra and Srinivas (1991) concluded from their experiments that Ergun's equation successfully predicts the pressure loss through packed beads for the creeping flow of shear-thinning fluids. Also, Shah and Yortsos (1995) used homogenization theory to show that a macroscopic law based on the single-capillary model applies to the single-phase flow of power-law fluids in porous media at low values of Reynolds number. Later, using stochastic homogenization, Fadili et al. (2002) presented a formula for up-scaling isotropic Darcy's flows of power-law fluids to heterogeneous Darcy's flows through. This formula expressed the importance of both rheological and porous medium related parameters on the mean flow and was in good agreement with numerical experiments. The same authors also proved the validity of the use of pore network models to describe flow of power-law fluids and used numerical simulations to validate the obtained expressions.

Other relevant issues concerning shear-thinning creeping flow in packed beds have also been addressed in the literature. On this subject, Rao and Chhabra (1993) studied the effects of column walls and particle size distribution on the flow rate–pressure drop relationship, proposing a wall correction method and confirming the applicability of the mean hydraulic radius of the particles to characterize a bed of mixed size spheres. Also, shear-thinning flow through non-spherical beads was successfully predicted by Machac et al. (1998) using two methods based on modifications of the capillary model. The impact of heterogeneity in porous medium properties is particularly relevant for non-Newtonian flow (Fadili et al., 2002; Longo et al., 2013; Di et al., 2014; Longo et al., 2015a; Longo et al., 2015b; Ciriello et al., 2016). In this respect, Gravity-driven non-Newtonian creeping flows were theoretically analyzed using self-similar solutions (backed by experiments) in the cases of radial flow in homogeneous (Longo et al., 2013) and stratified packed beds (Di et al., 2014), and two-dimensional flows in stratified packed beds (Ciriello et al., 2016).

Some shear-thinning fluids present other complex rheological behaviors such as yield stress or viscoelasticity, affecting flow through packed beds. Viscoelastic effects during the flow of shear-thinning polymer solutions in beds of particles was experimentally studied by Tiu et al. (1997), finding that the surface-mean particle diameter allows the correlation of pressure loss data using the existing equations for non-Newtonian purely viscous fluids. The creeping flow through packed beads of shear-thinning fluids having a yield stress was investigated by Chevalier et al. (2013). These authors obtained a general expression for the pressure drop vs. flow rate curve as a function of the rheological parameters of the fluid and the structural parameters of the porous medium. Then, by means of NMR measurements, Chevalier et al. (2014) provided insight into the physical origin of the coefficients involved in this general expression.

Only a few works have specifically addressed non-Darcian flow of shear-thinning fluids in packed beds. In this regard, some theoretical models were proposed that successfully predict the creeping and inertial flow of shear-thinning fluid through packed beds and granular media (Sabiri and Comiti, 1995; Smit and du Plessis, 1997), but the covered range of Reynolds number was limited. Other proposed models (Woudberg et al., 2006) showed important differences with the available experimental results at high Reynolds numbers, due to secondary order effects such as additional normal stresses that were not taken into account. Creeping and inertial flow experiments of shear-thinning fluids through beads of particles were conducted by Broniarz-Press et al. (2007), but the focus was on determining the minimum fluidization velocities for the beds. It should be noted that all the preceding studies involving non-Darcian fluid flow used the power-law model to represent the shear viscosity of the fluid. In this model, viscosity tends to zero at very high shear rate. Therefore, in spite of its practical interest in a number of applications, the power-law model does not provide a realistic value of viscosity at high shear rates as those involved in non-Darcian flow.

As can be deduced from the literature, the number of experimental works involving shear-thinning flow in which inertial effects are non-negligible is rather limited (Sabiri and Comiti, 1995; Chhabra et al., 2001; Broniarz-Press et al., 2007). Therefore, additional systematically performed experimental work is needed (Rao and Chhabra, 1993; Broniarz-Press et al., 2007), covering a wide range of *Re*, and specifically treating the shear-thinning flow through packed beads.

## 3. Materials and methods

### 3.1. Experimental setup and procedure

A set of experiments was conducted injecting aqueous polymer solutions through four packed beds formed by mono-size glass spheres. The diameter of the glass spheres $d_s$ was 1 mm, 3 mm, 4 mm and 5 mm in each case. The spheres were packed inside transparent Plexiglas columns with inner diameter $D = 5$ cm. Compact packings were achieved by shaking using vibratory sieve shaker.

The fluid was injected from a tank situated upstream of the porous column using a volumetric pump (EcoMoineau M Series, PCM, France), and its flow rate was measured with a positive displacement flow meter (Model LSM45, Oval, Japan). A differential pressure sensor (DP15 Variable Reluctance Pressure Sensor, Validyne, USA) was used to measure the pressure drop through the porous medium over a distance of $L = 20$ cm. The pump was able to provide flow rates ranging from 0 to 300 L/h, the range of the flow meter was from 7 to 500 L/h with an accuracy of ±1% and the range of the pressure sensor was adjusted by installing different membranes from 0–1400 Pa to 0–56,000 Pa with an accuracy of ±0.3% of the full scale. The injected fluid was continuously recirculated to the upstream tank after passing through the porous column. A photo showing the experimental setup is provided as Supplementary material. The columns were saturated with $CO_2$ (more water-miscible gas than air) prior to saturation with aqueous polymer solutions in order to avoid air trapping during the experiments. Once saturated with polymer solution, a set of twenty-six different flow rates ranging from 9 to 250 L/h were imposed for the flow through the porous medium and the corresponding pressure drops were measured. For each step, a fixed flow rate was maintained until the steady state pressure drop was reached. Each step was repeated four times and the uncertainty related to the repeatability of the pressure drop was calculated as $\pm 2\sigma$, with $\sigma$

=2% being an estimate of the relative standard deviation of the measurements (95% confidence interval). The room temperature during the experiments was 18 °C ± 1.

It can be observed that the range of $Q$ used in this work is significantly wider than those used in some preceding works (Sabiri and Comiti, 1995). This permits a better assessment of inertial effects, given that higher values of u are involved.

### 3.2. Fluid properties

Filtered water (polymer concentration $C_p = 0$ ppm) and three xanthan gum aqueous solutions with $C_p = 200$ ppm, $C_p = 500$ ppm and $C_p = 700$ ppm were used as injected fluids in the present experiments. Xanthan gum is a polysaccharide obtained through fermentation of Xanthomonas campestris bacteria. This biopolymer is widely used as viscosity-enhancing additive in the food and cosmetics industries, as zerovalent iron for groundwater remediation and as part of the formulation of drilling muds in EOR (Garcia-Ochoa et al., 2000; Amundarain et al., 2009; Palarinaj and Javarman, 2011; Wadhai and Dixit, 2011; Xin et al., 2015). Isolated xanthan macromolecules are known to be more or less rigid in solution state, with a contour length of typically 1 $\mu$m (Mongruel and Cloitre, 2003) and a transverse size of approximately 2 nm. Details on its chemical composition, structure and other physico-chemical properties can be found in Song (2007).

Sixty liters of each solution were prepared by progressively dissolving xanthan gum powders in filtered water containing 400 ppm of $NaN_3$ as a bactericide while gently mixing with a custom-made overhead device. Then, a stress controlled rheometer (ARG2, TA Instruments) equipped with cone-plate geometry was used to characterize the effective shear viscosity of the bulk fluids at a constant temperature of 18 °C ± 1, following a procedure previously presented in the literature (Rodríguez et al., 2014, 2016a, 2016b). A viscosity of 0.0011 Pa s was measured for the solvent (water) and the density $\rho$ of all injected fluids was taken as 1000 kg/m$^3$. The polymer solutions used herein were checked for possible mechanical degradation by collecting a set of effluent samples at the outlet of the porous media after injection at the highest flow rate. The rheograms of the effluents showed no significant difference with respect to those of the inflowing fluid, so polymer mechanical degradation was proved to be negligible. Moreover, no air macro bubbles were observed in the injected fluid. Also, the rheograms of a degassed fluid sample and an undegassed fluid sample were measured and compared in order to evaluate the influence of residual air micro bubbles, showing no significant difference.

The two-parameter power law model used in most of the preceding works (Chhabra and Srinivas, 1991; Rao and Chhabra, 1993; Sabiri and Comiti, 1995; Smit and du Plessis, 1997; Tiu et al., 1997; Machac et al., 1998; Chhabra et al., 2001; Broniarz-Press et al., 2007) is not appropriate to study non-Darcian flow as the involved shear rates are high and close to the upper Newtonian plateau of viscosity (Woudberg et al., 2006; Fayed et al., 2016). In contrast, the empirical Carreau model (Carreau, 1972) can accurately predict the variation in the viscosity at all shear rates and is known to successfully represent the shear-thinning behavior of xanthan gum semi-dilute solutions (Sorbie et al., 1989; López et al., 2003; Rodríguez et al., 2016a, 2016b). The Carreau equation is based on molecular network theory and is often presented as $\frac{\mu-\mu_\infty}{\mu_0-\mu_\infty} = [1+(\lambda\dot{\gamma})^2]^{\frac{n-1}{2}}$,where $\mu$ is the viscosity at a given shear rate $\dot{\gamma}$, $\mu_0$ and $\mu_\infty$ are the zero shear rate and infinite shear rate viscosities, respectively, $n$ is the power-law index, and $\lambda$ is the time constant. The values of $\mu_0$, $\mu_\infty$, $n$ and $\lambda$ are determined by the polymer concentration under given pressure and temperature conditions. In the region far from the low shear viscosity plateau, i.e. when $\dot{\gamma} \gg \frac{1}{\lambda}$, Carreau's law leads to the following expression (Rodríguez de Castro and Radilla, 2016):

$$\mu \approx \mu_\infty + (\mu_0 - \mu_\infty)\lambda^{n-1}\dot{\gamma}^{n-1} = \mu_\infty + a\dot{\gamma}^{n-1} \quad (8)$$

with $a = (\mu_0 - \mu_\infty)\lambda^{n-1}$. The flow experiments presented in the preceding subsection were conducted for all four polymer concentrations. For each value of $C_p$, a hundred and four measurements (four repetitions for each of the twenty-six flow rates) were carried out. The hundred and four measures for a given polymer concentration-porous column pair were considered to be an experimental set. All fluids were injected through the four packed beds, apart from the 700 ppm solution which was not injected through the porous column with $d_s = 1$ mm given that the high pressures generated were not adapted to the experimental setup. Therefore, a total of 1560 measurements (15 experimental sets) were executed.

## 4. Results and discussions

### 4.1. Non-Darcian flow of a Newtonian fluid: obtaining K, $\gamma$ and $\beta$ from experiments

The porosity $\varepsilon$ of each porous medium was measured from the difference in mass between the water-saturated column and the air-saturated column, excluding the dead volumes, and the obtained values are listed in Table 1. The uncertainty in the procedure of measuring the porosity was of ± 0.1%. It can be observed that the porosities of all used columns were close to the average value of 0.35, which is in good agreement with the values reported by Dukhan et al. (2014) and indicates that the glass spheres were compactly packed. The experimental sets of pressure gradient as a function of average velocity for water injection ($C_p = 0$ ppm) through each porous column are presented in Fig. 1. Permeability was calculated following a two-step procedure. First, the values of $K_j$ minimizing the sum $\sum_{i=1}^{j}(\nabla P_i - u_i\frac{\mu}{K_j})^2$were calculated for $j = 1\ldots N$ with $N$ being the number of experimental data and $\mu$ being the dynamic viscosity of water. Then, the value of $s$ ($s = 1\ldots N$) minimizing the quantity $\frac{\sum_{i=1}^{s}|\frac{\nabla P_i - u_i\frac{\mu}{K_s}}{\nabla P_i}|}{s}$ was determined and the corresponding $K_s$ value was selected as the permeability of the porous column. The obtained values of $K$ are presented in Table 1. As expected from Eq. (3), permeability increased for higher values of $d_s$.

Once permeability was determined, a standard least squares method was used to fit the ($u_i$, $\nabla P_i$, ) data to Forchheimer's law (Eq. (1)) and the values for $\beta$ were obtained. Then, the coefficients $A$ and $B$ of Ergun's equation (Eq. (2)) were determined by identifying the linear and quadratic terms of Eqs. (1) and (2), respectively. From $K$ and $\beta$, the value of $F$ was calculated in each case. The values of $\beta$, $A$, $B$ and $F$ are also presented in Table 1. It is noted that the obtained values for the drag coefficient $F$ are very close to those reported by Dukhan et al. (2014). These values of $F$ are not unique, which suggest a dependence of $F$ on $d_s$. This is in contrast to the existence of universal values for a given class of porous medium which was defended in some previous works (Hwang et al., 2002; Liu et al., 2006; Dukhan and Patel, 2011) and subsequently refuted (Dukhan et al., 2014). Although $F$ represents inertial effects and is sensitive to the roughness of the porous medium (Liu et al., 2006), significant variability in terms of roughness is not expected between the glass beads used in our work as they are all made of the same material. However, the relative roughness as reported to $d_s$ may change and have effect on $F$.

Fig. 1 shows that all the ($u_i$, $\nabla P_i$, ) data sets are well fitted by Forchheimer's law. Therefore, it can be deduced that viscous effects dominate the flow at the lowest flow rates while extra pressure losses due to inertial effects become important at moderate and high flow rates. Higher values of $\beta$ were found for smaller $d_s$.

**Table 1**
Porosity, permeability, Ergun parameters and inertial coefficients for the four packed beds. The expressed uncertainties correspond to 95% confidence interval.

| $d_s$(mm) | $\varepsilon$ | $K$ | $\beta$ | $F$ | $A$ | $B$ |
|---|---|---|---|---|---|---|
| 1 | 0.36 ± 0.1% | $5.9 \times 10^{-10}$ m$^2$ ± 2% | $2.3 \times 10^4$ m$^{-1}$ ± 1% | 0.55 ± 2% | $1.9 \times 10^2$ ± 3% | 1.6 ± 2% |
| 3 | 0.34 ± 0.1% | $5.1 \times 10^{-9}$ m$^2$ ± 6% | $6.3 \times 10^3$ m$^{-1}$ ± 1% | 0.45 ± 4% | $1.7 \times 10^2$ ± 7% | 1.2 ± 2% |
| 4 | 0.35 ± 0.1% | $9.5 \times 10^{-9}$ m$^2$ ± 7% | $4.1 \times 10^3$ m$^{-1}$ ± 1% | 0.40 ± 5% | $1.7 \times 10^2$ ± 8% | 1.1 ± 2 % |
| 5 | 0.34 ± 0.1% | $1.3 \times 10^{-8}$ m$^2$ ± 6% | $2.9 \times 10^3$ m$^{-1}$ ± 2% | 0.33 ± 4% | $1.8 \times 10^2$ ± 6% | 0.9 ± 2% |

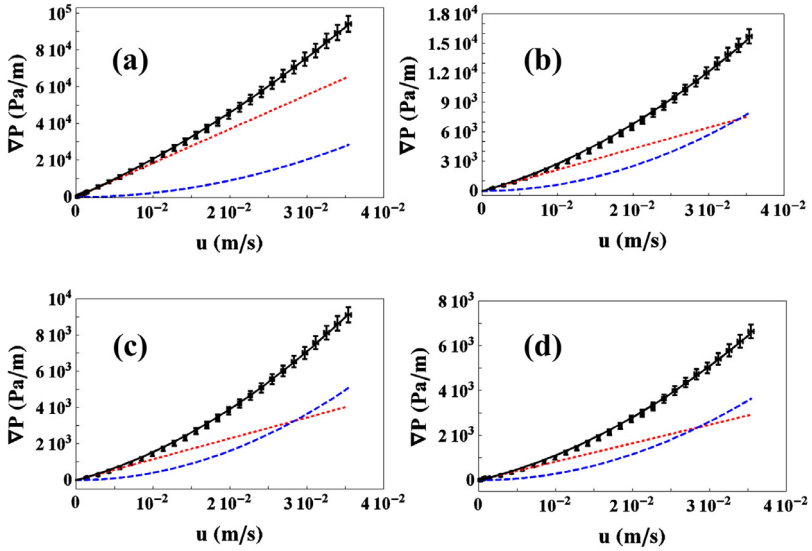


**Fig. 1.** Pressure gradient vs. average velocity for water injection through the packs of glass beads with (a) $d_s$ = 1 mm, (b) $d_s$ = 3 mm, (c) $d_s$ = 4 mm and (d) $d_s$ = 5 mm. Symbols represent experimental data, black solid lines represent their fit to Forchheimer's law, red dotted lines represent the linear term (Darcy's law), blue dashed lines represent the contribution of the quadratic term to the total pressure loss. (For interpretation of the references to color in this figure legend, the reader is referred to the web version of this article.)

**Table 2**
Parameters used in Eq. (8) for the shear rate–viscosity relations of the injected fluids. Uncertainties correspond to 95% confidence interval.

| $C_p$ (ppm) | $a$ (Pa s$^n$) | $n$ | $\mu_\infty$ (Pa s) |
|---|---|---|---|
| 200 | $4.8 \times 10^{-3}$ ±4% | $6.6 \times 10^{-1}$ ±1% | $1.1 \times 10^{-3}$ |
| 500 | $2.4 \times 10^{-2}$ ±5% | $5.8 \times 10^{-1}$ ±2% | $1.1 \times 10^{-3}$ |
| 700 | $4.2 \times 10^{-2}$ ±4% | $5.2 \times 10^{-1}$ ±1% | $1.1 \times 10^{-3}$ |

Nonetheless, the relative importance of the quadratic term of pressure loss increased as $d_s$ increased. Indeed, the Reynolds number at a given $u$ is higher for more permeable media, which explains that the inertial deviations from Darcy's law are more pronounced.

The average values of $A$ and $B$ obtained for our experiments were 170 and 1.2, respectively. The value of $A$ is comprised between the most commonly used values of 150 and 180. However, significant differences are found for $B$ with respect to the usual value of 1.75 (Ergun, 1952) and the range 1.8–4 proposed by Mac et al. (1979). These discrepancies were also reported by Dukhan et al. (2014) and may be the consequence of the wide range of $Re$ used in both studies.

### 4.2. Equivalent and shear viscosity relations

Eq. (8) was used to fit the experimental viscosity–shear rate data (Rodríguez et al., 2014, 2016a), which are presented as supplementary material, and the obtained values for $a$ and $n$ are presented in Table 2. On the basis of previously presented works, $\boldsymbol{\mu}_\infty$ was assumed to be that of the solvent (Bird et al., 1987; Pauchard et al., 1999; López, 2004; Saggin et Coupland, 2004; Auradou et al., 2008; Comba et al., 2011; Wengeler, 2014; Fang et al., 2015). The relative standard deviation of the shear rate measurements carried out with the rheometer for the determination of Carreau law parameters was ±1.5%.

As expected, higher viscosities were obtained for the most concentrated solutions used in the present study and the experimental data were well described by Eq. (8) using the parameters presented in Table 2. This table illustrates that a more pronounced shear-thinning behavior was obtained at high $C_p$, as reflected by the lower values of $n$.

Two approaches are commonly used to represent pressure loss data for the flow of non-Newtonian fluids through packed beads (Tiu et al., 1997). The first possibility involves the definition of apparent viscosity and shear rate in the porous medium. The second possibility lies in representing the correlation between $f$ and a properly defined $Re$. In this subsection, we will focus on the first approach while the second one will be treated in Section 4.5.

The inertial effects in the porous medium can be evaluated by comparing the shear viscosity calculated from effective viscosity measurements (using a rheometer) to the actually observed equivalent viscosity. The equivalent viscosity in the porous medium $\mu_{eq}$, in which both inertial and shear-thinning effects are included, can be defined from Darcy's law as (Tosco et al., 2013):

$$\mu_{eq} = -\frac{\nabla P}{u} K \tag{9}$$

Prior to calculation of the "in situ" apparent shear viscosity $\mu_{pm}$ in the porous medium, the apparent shear rate has to be determined. In the case of shear-thinning fluids, this apparent shear rate $\dot{\gamma}_{pm}$ can be defined by dividing the mean velocity $u$ by a characteristic microscopic length of the porous media (Chauveteau, 1982; Sorbie et al., 1989; Perrin et al., 2006; Tosco et al., 2013; Rodríguez et al., 2016a). This microscopic length is usually taken as $\sqrt{K\varepsilon}$ with

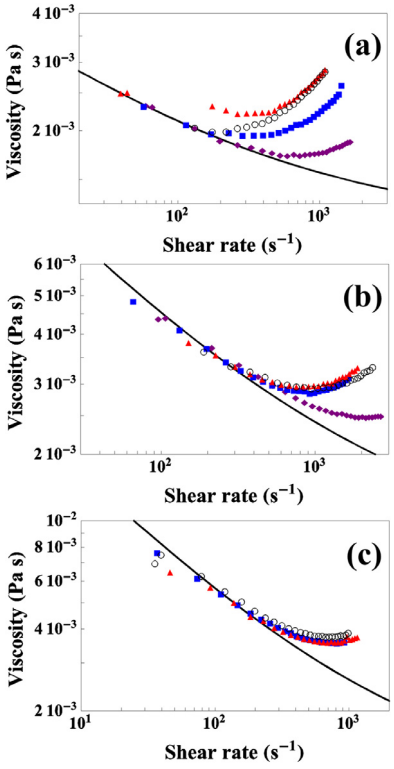


**Fig. 2.** $\mu_{eq}$ and $\mu_{pm}$ for the polymer concentrations of the injected fluid as a function of the glass beads diameter ($d_s$ = 1 mm with purple filled diamonds, $d_s$ = 3 mm with blue filled squares, $d_s$ = 4 mm with red filled triangles and $d_s$ = 5 mm in black empty circles). Symbols represent $\mu_{eq}$ and solid lines represent $\mu_{pm}$. (a) $C_p$ = 200 ppm, (b) $C_p$ = 500 ppm, (c) $C_p$ = 700 ppm. (For interpretation of the references to color in this figure legend, the reader is referred to the web version of this article.)

$\varepsilon$ being the porosity of the porous medium. Consequently, $\dot{\gamma}_{pm}$ can be defined as:

$$\dot{\gamma}_{pm} = \alpha \frac{u}{\sqrt{\varepsilon K}} \tag{10}$$

where $\alpha$ is a empirical shift factor. In the particular case of Carreau fluids, $\mu_{pm}$ can be obtained from Eqs. (8) and (10) as:

$$\mu_{pm} = \mu_\infty + a\left(\alpha \frac{u}{\sqrt{K\varepsilon}}\right)^{n-1} \tag{11}$$

In our experiments, $\alpha$ was determined for each porous medium-fluid pair by following the procedure proposed by Sorbie et al. (1988) and subsequently used by other authors (González et al., 2005; Amundarain et al., 2009). The procedure consisted in overlaying the porous media $\mu_{eq}$ vs. $\dot{\gamma}_{pm}$ curves with the bulk $\mu_{pm}$ vs. $\dot{\gamma}$ curves as closely as possible and noting the scale change in shear rate required to obtain the best fit. The results are shown in Fig. 2. It is noticed that overlaying $\mu_{eq}$ with $\mu_{pm}$ is more challenging at $C_p$ = 200 ppm, given that important inertial effects occur at lower shear rates as shown in this figure. Also, it should be noted that a good overlay between $\mu_{eq}$ and $\mu_{pm}$ curves is only possible in the low shear rates region where no significant inertial effects occur. This good overlay obtained at low shear rates shows that the effect of fluid-solid interactions (e.g. polymer mechanical degradation and apparent wall slip) on the relationship between viscosity and shear rate is negligible (González et al., 2005; Amundarain et al., 2009; Rodríguez et al., 2016a). This was expected given the small size of the polymer macromolecules (typically 1 $\mu$m) with respect to pore size. Moreover, all the computed values of $\alpha$ (see Table 3) lie in the interval 1–4.5, in agreement with literature data (Chauveteau, 1982; Sorbie et al., 1989; López, 2004; Comba et al., 2011). The average value obtained for $\alpha$ is 2, which is close to the universal value of 1.7 for packs of large spheres presented by Meurant (1981). However, a dependence of $\alpha$ on $d_s$ is observed in the present experiments in agreement with the results of Amundarain et al. (2009). Also, it should be noted that some previously reported correlations for the prediction of $\alpha$ were specifically developed for power-law fluids (Christopher and Middleman, 1965; Hirasaki and Pope, 1974; Cannella et al., 1988), so direct comparison is not possible as the impact of $\mu_\infty$ was not taken into account.

Fig. 2 shows that $\mu_{eq}$ vs. $\dot{\gamma}_{pm}$ curves are not monotonic in contrast to $\mu_{pm}$ vs. $\dot{\gamma}_{pm}$ curves. A decrease in $\mu_{eq}$ as $\dot{\gamma}_{pm}$ increases is observed at low shear rates, i.e. in the shear-thinning Darcy regime. However, the shear-thinning behaviur is compensated by inertial effects above a critical value of $\dot{\gamma}_{pm}$ in most cases, resulting in an increase in $\mu_{eq}$ as $\dot{\gamma}_{pm}$ increases in good agreement with the numerical experiments conducted by Tosco et al. (2013). A different behavior is remarked at the highest polymer concentration $C_p$ = 700 ppm, for which the increase in $\mu_{eq}$ at high shear rates is significantly less pronounced. In this case, a constant plateau of $\mu_{eq}$ is observed, which is explained by a strong shear-thinning behavior of the fluid even under high flow rates. These results suggest that $\mu_{eq}$ vs. $\dot{\gamma}_{pm}$ curves may be monotonically decreasing for greater values of $C_p$ in spite of the inertial effects within the considered range of shear rates. A similar behavior is observed in the cases $C_p$ =700 ppm and $C_p$ = 500 ppm for $d_s$ = 1 mm. Nevertheless, in these cases the observed plateau is explained by the less significant inertial effects in the porous column with $d_s$ = 1 mm. Consequently, it can be concluded that the inertial effects can be successfully compensated by shear-thinning effects for some combinations of $C_p$ and $d_s$. Moreover, it is highlighted that the inertial regime occurs at high flow rates that lie in the region close to the upper Newtonian plateau of viscosity where the shear-thinning behavior is moderate.

From Eqs. (1) and (9), the following expression can be deduced:

$$\mu_{eq} = \mu_{pm} + \beta K \rho u = \mu_{pm} + \frac{\beta K^{3/2} \varepsilon^{1/2} \rho \dot{\gamma}}{\alpha} \tag{12}$$

Fig. 2 shows that in the case $C_p$=200 ppm, $\mu_{eq}$ increases from $d_s$ =1 mm to $d_s$ = 3 mm and from $d_s$ = 4 mm to $d_s$ = 5 mm, while it remains practically unchanged from $d_s$ = 4 mm to $d_s$ = 5 mm. This may be explained by observing from Eq. (12) that the factor $\frac{\beta K^{3/2}}{\alpha}$ determines the deviation of $\mu_{eq}$ with respect to $\mu_{pm}$. It is noted that the higher values of $\alpha$ obtained for high values of $d_s$ attenuate the increase in inertial effects for the most concentrated polymer solutions. Indeed, this factor $\frac{\beta K^{3/2}}{\alpha}$ increases from $d_s$ = 1 mm to $d_s$ = 4 mm but does not significantly change from $d_s$ = 4 mm to $d_s$ = 5 mm (see Tables 2 and 3). For the same reason, no significant difference was found in terms of $\mu_{eq}$ between $d_s$ = 3 mm and $d_s$ = 5 mm for $C_p$ = 500 ppm and $C_p$ = 700 ppm.

The range of variation of $\mu_{eq}$ increases as $C_p$ increases for all porous columns. This is a consequence of the higher degree of shear-thinning presented by the most concentrated solutions. However, the high levels of $\mu_{eq}$ observed at low shear rates in the particular case of $C_p$ = 200 ppm and $d_s$ = 4 mm may be related to inaccuracies in the measurements due to proximity to the range limits of the used pressure sensors and will need further study.

### 4.3. Polymer concentration effects on Reynolds number

It is known that Reynolds numbers is directly proportional to injection flow rate for Newtonian fluids. However, a different behavior occurs when using shear-thinning fluids. Indeed, according to Eq. (11), increasing the flow rate implies a decrease in

**Table 3**
Apparent-to-effective viscosity shift factor $\alpha$ for the shear rate–viscosity relations shown in Fig. 2.

| $C_p$ (ppm) | $\alpha$ ($d_s$ = 1 mm) | $\alpha$ ($d_s$ = 3 mm) | $\alpha$ ($d_s$ = 4 mm) | $\alpha$ ($d_s$ = 5 mm) |
|---|---|---|---|---|
| 200 | 0.7 | 1.7 | 1.8 | 2.1 |
| 500 | 1.1 | 2 | 3.1 | 4.5 |
| 700 | – | 1.1 | 1.9 | 1.9 |

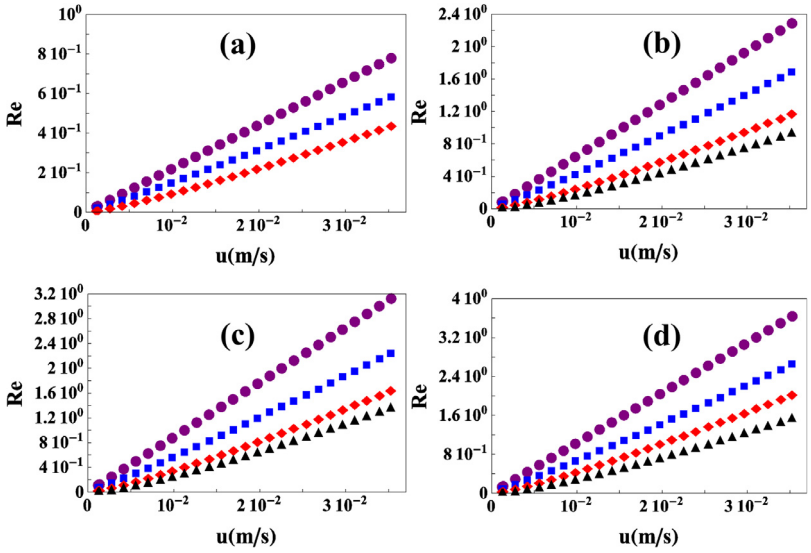


**Fig. 3.** (a) *Re* vs. *u* as a function of $C_p$ for the packs of glass beads with (a) $d_s$ = 1 mm, (b) $d_s$ = 3 mm, (c) $d_s$ = 4 mm and (d) $d_s$ = 5 mm. Different colors represent different polymer concentrations: $C_p$ = 0 ppm in purple, $C_p$ = 200 ppm in blue, $C_p$ = 500 ppm in red and $C_p$ = 700 ppm in black. (For interpretation of the references to color in this figure legend, the reader is referred to the web version of this article.)

**Table 4**
Average relative errors *E* resulting from the fit of *Re* as a function of *u* using a linear model.

| $C_p$ (ppm) | $d_s$ = 1 mm (%) | $d_s$ = 3 mm (%) | $d_s$ = 4 mm (%) | $d_s$ = 5 mm (%) |
|---|---|---|---|---|
| 0 | 0 | 0 | 0 | 0 |
| 200 | 8 | 9 | 9 | 9 |
| 500 | 23 | 27 | 26 | 24 |
| 700 | – | 46 | 43 | 45 |

$\mu_{pm}$which implies in turn an extra increase in Reynolds number (Eq. (5)). This behavior can be observed in Fig. 3, where *Re* is presented as a function of u. Indeed, one can remark that while Reynolds number is a linear function of u for $C_p$ = 0 ppm, this is not the case for higher concentrations. The average relative errors *E* resulting from the fit of Reynolds as a function of u using a linear model were calculated in each case as $E = \frac{\sum_{j=1}^{N} \frac{|fit(u_j) - Re_j|}{Re_j}}{N}$,with *N* being the number of experimental data. These average errors are shown in Table 4 for the four porous media.

In Fig. 3, it can also be observed that *Re* decreases as $C_p$ increases for a given flow rate. Also, the range of *Re* corresponding to the range of imposed flow rates is narrower as $C_p$ increases, due to the higher viscosities of the most concentrated solutions. In contrast, the ranges and values of *Re* increase as $d_s$ increases, given the higher values of *u*.

Depending on the value of the interstitial Reynolds number defined as $Re_i = \frac{\rho u d_s}{\mu_{pm}\varepsilon}$, Dybbs and Edwards (1984) postulated the existence of four different flow regimes: (1) the Darcy or creeping flow regime for $Re_i < 1$ where viscous forces dominate and the velocity distribution is determined by local geometry. (2) The inertial regime beginning at $1 < Re_i < 10$ and extending up to $Re_i \sim 150$ characterized by a more pronounced boundary layer and the existence of an "inertial core" . (3) The unsteady laminar flow regime for $150 < Re_i < 300$, characterized by the formation of waves. (4) The highly unsteady and chaotic flow regime for $Re_i > 300$, analogous to turbulent flow in pipes and dominated by eddies. However, disagreement exists regarding the criteria for transition among flow regimes (Chhabra et al., 2001; Dukhan et al., 2014).

**Table 5**
Range of interstitial Reynolds numbers $Re_i$ covered in each experiment as a function of $d_s$ and $C_p$.

| $d_s$ (mm) | $C_p$ = 0 ppm | $C_p$ = 200 ppm | $C_p$ = 500 ppm | $C_p$ = 700 ppm |
|---|---|---|---|---|
| 1 | 3.3–90.3 | 1.5–60.8 | 0.8–50.6 | – |
| 3 | 10.1–281 | 4.7–205.1 | 2.1–143.2 | 1.3–116.5 |
| 4 | 13.2–367.2 | 5.8–261.3 | 2.8–192.4 | 1.8–162 |
| 5 | 16.9–469.8 | 7.5–334.2 | 3.9–257.2 | 2.2–198.6 |

The range of $Re_i$ explored by the present experiments are listed in Table 5, showing that all flow regimes are covered according to the criteria presented by Dybbs and Edwards (1984), in contrast to previously presented experimental studies for shear-thinning flow in packed beads (e.g. Chhabra and Srinivas, 1991; Rao and Chhabra, 1993). Therefore, the efficiency of Forchheimer's law and Ergun's equation to represent the flow rate–pressure drop relationships in all regimes can be better assessed with the present experimental data.

**Table 6**
Average errors, median errors and standard deviation of the errors obtained for the three methods used to predict $\Delta P$ as a function of $u$ from Ergun's equation.

| Prediction method | Average error (%) | Median error (%) | Standard deviation error (%) |
|---|---|---|---|
| Method 1 | 19 | 18 | 12 |
| Method 2 | 11 | 8 | 14 |
| Method 3 | 5 | 4 | 9 |

### 4.4. Predicting the relationship between u and ΔP for shear-thinning fluids using Ergun's equation

Predicting the pressure drop for the inertial flow of shear-thinning fluids through unconsolidated porous media is of vital importance in several applications, as mentioned in the introduction of this article. To do so, three different approaches are used in this subsection and their results are compared to the experimental data. The choice of a particular approach will be motivated by the amount of available information at the preliminary stage and the expected accuracy for the prediction.

#### 4.4.1. Predicting the relationship between u and ΔP using Ergun's equation with universal empirical constants for a and b and a unique shift factor $\boldsymbol{\alpha}$

In this first approach (Method 1), only the effective shear rheology of the fluid ($\mu_\infty$, $a$, $n$), the porosity of the porous medium and the sphere size are needed for the calculation. In the original form of Ergun's equation (Ergun, 1952), universal values of $A = 150$ and $B = 1.75$ were used in Eq. (2). Moreover, Meurant (1981) proposed a unique shift factor $\alpha = 1.7$ for packs of large spheres having the same diameter. If the preceding values are used in Eqs. (2) and (11), the following relationship between $u$ and $\Delta P$ is obtained:

$$\Delta P = 150\frac{(1-\varepsilon)^2\left[\mu_\infty + a\left(1.7\frac{6\sqrt{5}(1-\varepsilon)u}{\varepsilon^2 d_s}\right)^{n-1}\right.}{\varepsilon^3 d_s^2}uL + \frac{1.75}{\varepsilon^3}\frac{(1-\varepsilon)\rho}{d_s}u^2L \tag{13}$$

To evaluate the accuracy of the proposed methods for the pressure drop predictions, the average relative deviations of predicted data with respect to experimental data $\delta$ were calculated as $\delta = \frac{1}{N}\sum_{i=1}^{N}\delta_i$ with $\delta_i = |1 - \frac{(\Delta P_{calc})_i}{(\Delta P_{exp})_i}|$ (Sabiri and Comiti, 1995; Machac et al., 1998). The resulting average and mean errors for this first method are summarized in Table 6 together with the standard deviations. Also, the comparison between the predictions made using this approach and the experimental data obtained from our experiments is presented in Fig. 4. As can be observed in this figure, important differences exist between predicted and experimental values. These differences may be explained, in part, by the universal value of $B = 1.75$ used in the calculations, which differs from the average value of $B = 1.18$ obtained by fitting the present experimental data as mentioned in Section 4.1. In fact, if the universal value of $B = 1.18$ is used instead of $B = 1.75$, the resulting average error is reduced from 18.5% to 12.0%.

#### 4.4.2. Predicting the relationship between u and ΔP from non-Darcian water flow experiments using Ergun's equation and a unique shift factor $\boldsymbol{\alpha}$

This second approach (Method 2) consists in using the values of $A$ and $B$ obtained from water injection experiments in each porous medium (listed in Table 2) instead of the universal values mentioned in the preceding section. No information from shear-thinning fluid injection is needed in this approach and a unique value of $\alpha = 1.7$ (Meurant, 1981) is used for the shift factor. The resulting expression for the calculation of $\Delta P$ is:

$$\Delta P = A\frac{(1-\varepsilon)^2\left[\mu_\infty + a\left(1.7\frac{6\sqrt{5}(1-\varepsilon)u}{\varepsilon^2 d_s}\right)^{n-1}\right.}{\varepsilon^3 d_s^2}uL + B\frac{(1-\varepsilon)\rho}{\varepsilon^3 d_s}u^2L \tag{14}$$

Experimental and predicted data using this method (Method 2) are also presented in Fig. 4, showing good agreement in most cases. A worse agreement is obtained in those cases in which the value of $\alpha$ is not close to 1.7 (see Table 3). The resulting errors are also summarized in Table 6. These errors are considerably lower than those obtained by using the preceding approach and may be acceptable in many cases.

#### 4.4.3. Predicting the relationship between u and ΔP from non-Darcian water flow and Darcian shear-thinning flow experiments using Ergun's equation

This last approach (Method 3) to predict the relationship between u and $\Delta P$ does not involve the use of any universal value. Indeed the used values for $A$ and $B$ are obtained from non-Darcian flow experiments with water (Table 2) and the values of $\alpha$ are obtained from the Darcian flow region of the shear-thinning flow experiments (Table 3). The preceding inputs can be used in the following expression to predict pressure drop of shear-thinning flow at any flow rate:

$$\Delta P = A\frac{(1-\varepsilon)^2\left[\mu_\infty + a\left(\alpha\frac{6\sqrt{5}(1-\varepsilon)u}{\varepsilon^2 d_s}\right)^{n-1}\right.}{\varepsilon^3 d_s^2}uL + B\frac{(1-\varepsilon)\rho}{\varepsilon^3 d_s}u^2L \tag{15}$$

The obtained predictions are compared to the experimental data in Fig. 5, showing good agreement. Also in the case of this Method 3, the resulting errors were calculated and are presented in Table 6, showing a reduction of more than 50% with respect to Method 2. The errors obtained from Method 3 are lower than those presented by Sabiri and Comiti (1995) and Machac et al. (1998). Also, these results are in sharp contrast with the conclusions of the work presented by Mac et al. (1979), which stated that Ergun's equation predicts the values of pressure drop with an uncertainty of ±50% for unconsolidated media in most cases of practical interest. It is worth noting that the calculated errors must not be completely attributed to inaccuracies in the prediction methods, but they may be explained in part by the uncertainties inherent to the performed measurements and the fitting process to experimental data, as explained above. Also, it is remarked that wall effects in the porous column have not been taken into account. However, these have been shown to be less significant in the case of shear-thinning fluids (Rao and Chhabra, 1993).

It is reminded that Ergun's equation empirical parameters were obtained in Section 4.1. through identification from Forchheimer's equation. Therefore, all the results presented in this section for Ergun's equation also apply for Forchheimer's equation. An important consequence of these findings is that Forchheimer's law can be extended to the case of shear-thinning fluids. Also, elongational viscosity effects have been shown to be negligible in the case of the present experiments, given that the total pressure drop can be fully explained in terms of the addition of shear and inertial effects.

### 4.5. Effects of polymer concentration on the inertial contribution to total pressure loss and on the relationship between f and 1/Re

The total pressure loss can be presented as the sum of the inertial and shear contributions, $\Delta P_{inertial}$ and $\Delta P_{shear}$ , respectively

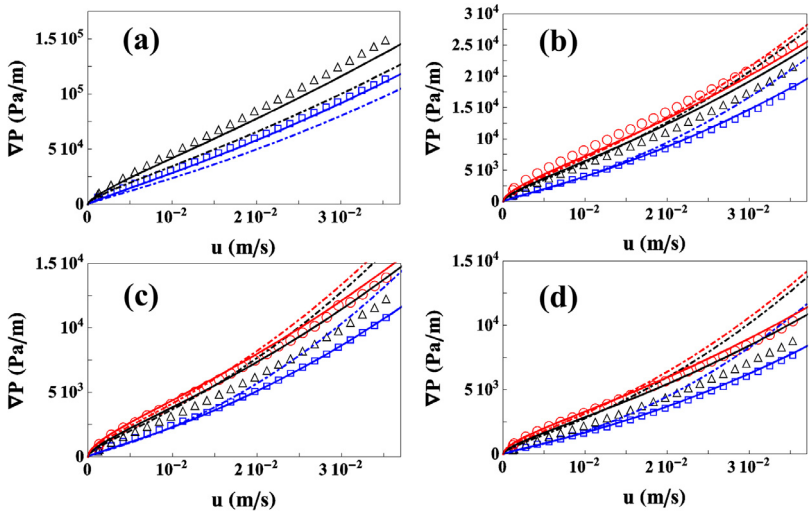


**Fig. 4.** $\nabla P$ as a function of u for all the values of $d_s$ and $C_p$ involved in the present experiments. (a) $d_s = 1$ mm, (b) $d_s = 3$ mm, (c) $d_s = 4$ mm and (d) $d_s = 5$ mm. Symbols represent experimental data. Dot-dashed lines represent predictions using Method 1 and solid lines represent predictions using Method 2. Different colors represent different polymer concentrations: $C_p = 200$ ppm in blue, $C_p = 500$ ppm in black and $C_p = 700$ ppm in red. (For interpretation of the references to color in this figure legend, the reader is referred to the web version of this article.)

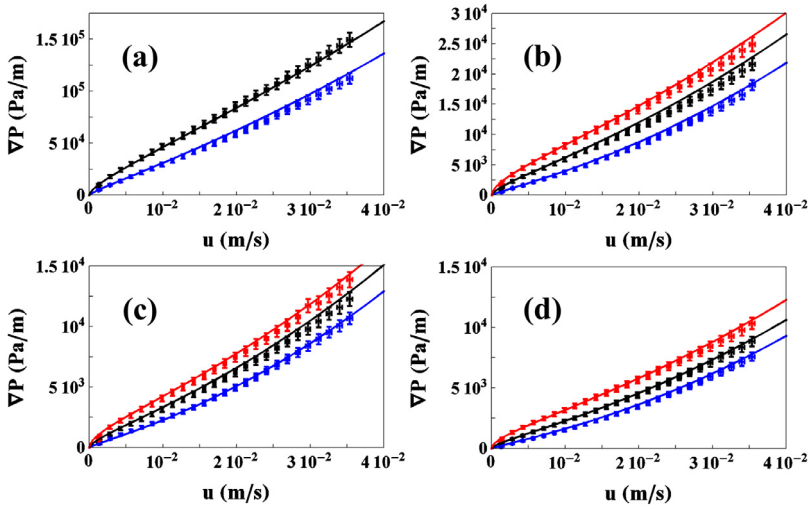


**Fig. 5.** $\nabla P$ vs. $u$ as a function of $C_p$ for the packs of glass beads with (a) $d_s = 1$ mm, (b) $d_s = 3$ mm, (c) $d_s = 4$ mm and (d) $d_s = 5$ mm. Symbols represent experimental data and solid lines represent predictions using Method 3. Different colors represent different polymer concentrations: $C_p = 200$ ppm in blue, $C_p = 500$ ppm in black and $C_p = 700$ ppm in red. (For interpretation of the references to color in this figure legend, the reader is referred to the web version of this article.)

(González et al., 2005; Tosco et al., 2013; Fourar et al., 2004):

$$\Delta P_{total} = \Delta P_{shear} + \Delta P_{inertial} \tag{16}$$

Forchheimer number $F_0$ is defined (Ruth and Ma, 1992; Dukhan et al., 2014) as the ratio between $\Delta P_{inertial}$ and $\Delta P_{shear}$ predicted by Forchheimer's law (Eq. (1)):

$$F_0 = F\ \frac{\rho u\sqrt{K}}{\mu} = F\ Re \tag{17}$$

It is reminded here that F is the experimentally determined inertial coefficient in Forchheimer's equation (Eq. (1)). $F_0$ is presented as a function of *Re* for each porous column in Fig. 6. This figure shows that for all packed beds, the data points corresponding to all values of $C_p$ collapse on the same master curve. Therefore, it can be deduced that $C_p$ does not affect the importance of inertial pressure loss for a given value of *Re*. Moreover, these results illustrate that higher values of $\beta$ (see Table 2) do not necessarily entail more significant inertial effects in relative terms as mentioned in Section 4.1.

Two types of criteria, the critical *Re* number and the critical $F_0$, have been proposed in the literature to identify the onset of non-Darcian flow. A review on these criteria was presented by Zeng and Grigg (2006). In the present study, inertial effects will be considered to be significant only above $F_0 = 0.1$, i.e. when $\Delta P_{inertial}$ is higher than 10% of $\Delta P_{shear}$. It can be observed in Fig. 6 that the value of *Re* for which $F_0 = 0.1$ does not depend on $C_p$ and is close to 0.2 in all cases (comprised between 0.1 and 0.3 depending on the porous medium). Comparison with the literature in terms critical *Re* is challenging due to the different definitions and criteria used by different researchers. For this reason the choice of a critical value of $F_0$ instead of a critical value of *Re* for the transition between Darcian and non-Darcian regime was preferred, in agreement with Zeng and Grigg (2006).

The values of $1/Re$ and f (Eq. 4) corresponding to each experimental ($Q_i$, $\nabla P_i$, ) data set were calculated and are provided as Supplementary material. Moreover, the water injection experimental data were fitted to Eq. (6) and the obtained values for the coefficients a and b were named $a_w$ and $b_w$, respectively, and are listed in Table 7 as a function of $d_s$. The values of $a_w$ are very close to

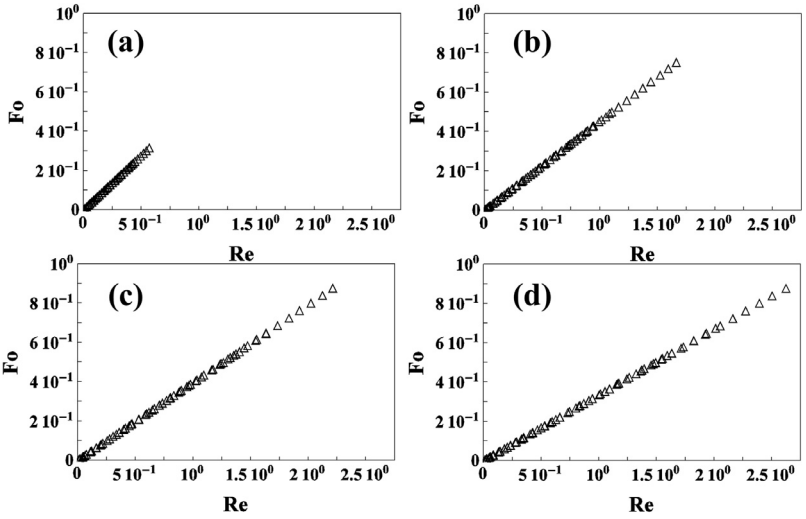


**Fig. 6.** $F_0$ vs. $Re$ for the packs of glass beads with (a) $d_s = 1$ mm, (b) $d_s = 3$ mm, (c) $d_s = 4$ mm and (d) $d_s = 5$ mm. Symbols represent experimental data corresponding to all values of $C_p$.

**Table 7**
Values of the coefficients obtained by fitting the experimental data of $f$ vs. $1/Re$ to Eq. (6). The coefficients corresponding to the fit of water data are named $a_w$ and $b_w$. The coefficients resulting from the fit of the whole data set encompassing all $C_p$ for a given $d_s$ are named $a_{all}$ and $b_{all}$. The last row shows the values obtained by fitting together the experimental data of the four porous columns. The values of $F$ for each porous column are also listed for comparison between Eqs. (6) and (7). The expressed uncertainties correspond to 95% confidence interval.

| $d_s$ (mm) | $a_w$ | $b_w$ | $a_{all}$ | $b_{all}$ | $F$ |
|---|---|---|---|---|---|
| 1 | $9.8 \times 10^{-1} \pm 2\%$ | $5.5 \times 10^{-1} \pm 8\%$ | $9.9 \times 10^{-1} \pm 1\%$ | $5.1 \times 10^{-1} \pm 8\%$ | $0.55 \pm 2\%$ |
| 3 | $7.7 \times 10^{-1} \pm 5\%$ | $5.8 \times 10^{-1} \pm 7\%$ | $9.0 \times 10^{-1} \pm 2\%$ | $4.9 \times 10^{-1} \pm 5\%$ | $0.45 \pm 4\%$ |
| 4 | $7.8 \times 10^{-1} \pm 3\%$ | $4.9 \times 10^{-1} \pm 3\%$ | $8.7 \times 10^{-1} \pm 3\%$ | $4.6 \times 10^{-1} \pm 7\%$ | $0.40 \pm 5\%$ |
| 5 | $7.7 \times 10^{-1} \pm 1\%$ | $4.0 \times 10^{-1} \pm 2\%$ | $8.7 \times 10^{-1} \pm 3\%$ | $3.8 \times 10^{-1} \pm 6\%$ | $0.33 \pm 4\%$ |
| All | $9.0 \times 10^{-1} \pm 4\%$ | $4.1 \times 10^{-1} \pm 8\%$ | $9.3 \times 10^{-1} \pm 2\%$ | $3.9 \times 10^{-1} \pm 4\%$ | |

those reported by Dukhan et al. (2014) for their experiments with $d_s = 1$ mm ($a_w = 1$) and $d_s = 3$ mm ($a_w = 0.7692$). However, this is not the case for the values of $b_w$, possibly due to differences in the roughness of the used porous media. The fits obtained by Dukhan et al. (2014) are also shown in the supplementary figure for comparison.

It is noted that only the results corresponding to $d_s = 1$ mm are well fitted by Eq. (7), and values of $a_w$ smaller than unit are obtained in the other cases. This remark is not trivial and can be explained by the fact that the f-$Re$ data corresponding to Darcian and non-Darcian flow regimes were fitted together. By doing so, a contribution to f is artificially attributed to inertial effects in the Darcian region, which results in underestimation of coefficient a. Rigorously speaking, the value of coefficient a in Eq. (6) should be obtained by fitting the $f$–$Re$ data in Darcian region to the relationship $f = a/Re$, which results in values of parameter a close to unit. However, the present approach was followed in order to facilitate comparison with previously published data. This underestimation of parameter $a$ in Eq. (6) leads to overestimation of parameter $b$. Consequently, the obtained values of $b_w$ are greater than $b_w = F$ predicted by Eq. (7). Also, the experimental $f$–$Re$ data corresponding to all $C_p$ were fitted together to Eq. (6), obtaining the values $a = a_{all}$ and $b = b_{all}$ listed in Table 7. It is observed that $a_{all} > a_w$ and $b_{all} > b_w$ in all cases, which is explained by the higher concentration of experimental data in the Darcian region for $C_p > 0$ ppm which reduce the underestimation of the parameter a.

The whole experimental data of $f$ vs. $1/Re$ encompassing all values of $C_p$ and $d_s$ used in this work are presented together in Fig. 7. It can be observed that all data sets collapse on the same master curve, which shows that the relationship between $f$ and $Re$ does

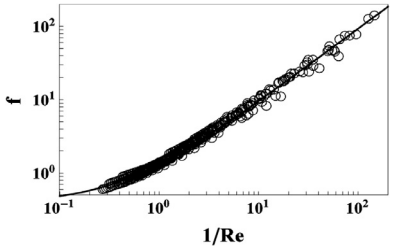


**Fig. 7.** Friction factor vs.$1/Re$ for all the fluid-packed bed combinations used in this work. Symbols represent experimental data. Solid lines represent the fit of all experimental data to Ergun's equation: (Eq. (2) using $a = 9.3 \times 10^{-1}$ and $b = 3.9 \times 10^{-1}$).

not depend either on $d_s$ or $C_p$ for the fluids and porous media used in this work. Therefore, the value of f can be predicted through Eq. (6) by using the values of $a = 9.3 \times 10^{-1}$ and $b = 3.9 \times 10^{-1}$ ($a_{all}$ and $b_{all}$ in the last row of Table 7) whatever the fluid and the porous media. Also, it is highlighted that even if some of the present experimental data would correspond to turbulent regime according to the criteria presented by Dybbs and Edwards (1984) (see Table 5), no constant plateau of $F$ (characteristic of turbulent regime) is observed at high values of $Re$ in Fig. 7. This suggests that turbulent regime is not fully developed in any of the present experiments.

Comparison of our $Re$–$f$ results with other works previously presented in the literature is challenging for two reasons. First, the characteristic length used in the definition of $Re$ differs from one work to another ($\sqrt{K}$ instead of, for example $d_s$, is used here).

Second, the previously presented definitions often rely on power law rheological model, while a Carreau model is used here. Therefore, it is tricky to compare the range of *Re* involved in each study. However, it is noticed that most previous works involve only the viscous flow without inertial effects. Also, as can be observed in Fig. 7, Ergun's equation successfully predicts the relationship between $f$ and $Re$ for the full range of $Re$ used in this work, in contrast to some works previously presented (Broniarz-Press et al., 2007). Moreover, in contrast to previously presented results for viscoelastic polymer solutions (Tiu et al., 1997), the total pressure drop can be attributed to addition of shear and inertial contributions. As mentioned in the preceding subsection, elongational viscosity did not produce any significant effect in the present experiments in contrast to the works of Amundarain et al. (2009). However, comparison of the results is not evident given the different definition of $Re$ used by the latter authors.

## 5. Summary and conclusions

The main goal of this article is to assess the efficiency of the most popular equations used to predict pressure drop–flow rate relationship for non-Darcian flow regime in the case of shear-thinning fluids injected through unconsolidated porous media. To do so, a realistic model to represent the rheology of commonly encountered shear-thinning fluids such as aqueous polymer solutions is combined with Forchheimer's law and Ergun's equation and three different approaches are proposed to predict pressure drop during inertial flow in packed beds of glass spheres. Each of these approaches requires a different number of inputs which determine the accuracy of the obtained predictions. A set of 1560 experimental flow rate–pressure drop measurements is then used to systematically evaluate the accuracy of the proposed prediction methods as a function of the rheology of the injected fluids (determined by the polymer concentration) and the size of the glass spheres.

In our study, the permeability and inertial coefficients of each porous medium were first determined from inertial flow experiments with water (Newtonian fluid). Then, the shift factors $\alpha$ between apparent and effective viscosities were obtained from Darcian flow of shear-thinning fluids. At this stage, the deviations of the predicted shear viscosity from the actually observed viscosity during the flow in the porous media allowed us to evaluate the importance of inertial effects. In contrast to the monotonically decreasing $\mu_{pm}$ vs. $\dot{\gamma}_{pm}$ curves, $\mu_{eq}$ was found to increase above a critical value of $\dot{\gamma}_{pm}$ for the lowest values of $C_p$. A $\mu_{eq}$ plateau was observed for the highest $C_p$. This results from competition between the shear-thinning viscosity of the injected fluids and the extra pressure losses arising from inertial effects. Based in our results, we have shown that a macroscopic law including rheological parameters of the fluid and structural parameters of the porous medium (Eqs. (13)–(15) can be used to predict non-Darcian flow of Carreau fluids in packed beds, analogously to the results of Chevalier et al. (2014) for yield stress and power-law fluids. As mentioned above, the use of power-law model is not convenient in the present study, given that this model predicts that viscosity tends to zero at very high shear rates as those involved in our experiments.

In the first proposed method, only $\varepsilon$, $d_s$ and the effective shear rheology of the fluid ($\mu_\infty$, $a$, $n$) were used as inputs for the $\Delta P$ predictions, obtaining an average relative error of 18.5%, which was reduced to 11.2% by adding the inertial coefficients coming from water injection in the second method. As expected, the most accurate predictions (relative error of 5.4%) were obtained by the third method in which the $\alpha$ shift factor determined through Darcian shear-thinning flow experiments was also used as input. These results prove that Ergun's equation successfully predicts the pressure drop for the injection of shear-thinning fluids in packed beads as well as the applicability of Forchheimer's law to shear-thinning fluids as long as a realistic model for shear viscosity is used.

An experimental protocol to predict flow rate–pressure drop relationships for the non-Darcian flow of shear-thinning fluids through packs of glass spheres is proposed:

(1) Determine the porosity of the porous medium and measure the effective shear rheology of the fluid ($\mu_\infty$, $a$, $n$).
(2) Determine the accuracy goal for the prediction flow rate–pressure drop relationships.
  2.1 If a relative error of the order of 20% is acceptable for the considered application, use Eq. (13).
  2.2 If a relative error smaller than 20% is necessary, perform water injection experiments to determine the values of $A$ and $B$.
    2.2.3 If a relative error of the order of 10% is acceptable, use Eq. (14).
    2.2.4 If a relative error of the order of 5% is needed, perform Darcian flow experiments with the involved fluid in order to determine the value of $\alpha$ and then use Eq. (15).

It has to be remarked that the expected accuracy levels are only based on the average values obtained in the present experiments, so they should be reassessed in the case of different experimental setups or working conditions. The proposed methods, each of them having a variable number of inputs, can be implemented in chemical flood simulation software for soil remediation and EOR in order to improve the accuracy of the $Q$ vs. $\Delta P$ predictions at the pilot plant and reservoir scales. Indeed, the obtained results can provide guidance on the choice of the preliminary laboratory experiments needed to obtain the inputs for the prediction of $\Delta P$ with a given accuracy.

It has been shown that addition of xanthan gum biopolymer to water reduces the relative importance of the inertial contribution to total pressure loss. This suggests that the inertial pressure loss may be neglected without leading to important errors in the predictions of total pressure loss for the injection of highly concentrated polymer solutions. Also, all the experimental data were found to collapse on the same $f$ vs. $1/Re$ master curve, independently of the fluid's shear rheology and the value of $d_s$, provided that a proper definition of Reynolds number and friction factor are used.

Moreover, criteria for the choice of the fluid's shear rheology can also be deduced from the present work. Our findings must now be extended to other types of porous media, such as bisized and consolidated porous media. Also, fully developed turbulent regime should be covered in future works and the case of commonly encountered viscoelastic shear-thinning fluids has to be investigated.

## Acknowledgments

The authors would like to thank Frédéric Bastien for his assistance with the experimental setup.

## Supplementary materials

Supplementary material associated with this article can be found, in the online version, at doi:10.1016/j.advwatres.2016.12.009.

## References

Antohe, B.V., Lage, J.L., Price, D.C., Weber, R.M., 1996. Numerical characterization of micro heat exchangers using experimentally tested porous aluminium layers. Int. J. Heat Fluid Flow 17, 594–603.

Amundarain, J.L., Castro, L.J., Rojas, M.R., Siquier, S., Ramírez, N., Müller, A.J., Sáez, A.E., 2009. Solutions of xanthan gum/guar gum mixtures: shear rheology, porous media flow, and solids transport in annular flow. Rheol. Acta 48, 491–498.

Auradou, H., Boschan, A., Chertcoff, R., Gabbanelli, S., Hulin, J.P., Ippolito, I., 2008. Enhancement of velocity contrasts by shear-thinning solutions flowing in a rough fracture. J. Non Newton. Fluid Mech. 153, 53–61.

Beavers, G.S., Sparrow, E.M., Rodenz, D.E., 1973. Influence of bed size on the flow characteristics and porosity of randomly packed beds of spheres. ASME J. Appl. Mech. 40, 655–660.

Bird, R.B., Armstrong, R.C., Hassager, O., 1987. Dynamics of Polymeric Liquids vol. 1: Fluid Dynamics, second ed. Wiley, New York.

Boomsma, K., Poulikakos, D., 2002. The effect of compression and pore size variations on the liquid flow characteristics in metal foams. J. Fluids Eng. 124, 263–272.

Broniarz-Press, L., Agacinski, P., Rozanski, J., 2007. Shear-thinning fluids flow in fixed and fluidized beds. Int. J. Multiph. Flow 33, 675–689.

Cannella, W.J., Huh, C., Seright, R.S., 1988. Prediction of xanthan rheology in porous media. In: Proceedings of the SPE Annual Technical Conference and Exhibition. Houston, Texas.

Carreau, P.J., 1972. Rheological equations from molecular network theories. Trans. Soc. Rheol. 16, 99–127.

Chhabra, R.P., Comiti, J., Machac, I., 2001. Flow of non-Newtonian fluids in fixed and fluidised beds. Chem. Eng. Sci. 56, 1–27.

Chhabra, R.P., Srinivas, B.K., 1991. Non-Newtonian (purely viscous) fluid flow through packed beads: effect of particle shape. Powder Technol. 67, 15–19.

Chauveteau, G., 1982. Rodlike polymer solution flow through fine pores: influence of pore size on rheological behavior. J. Rheol. 26, 111.

Chauveteau, G., Thirriot, C., 1967. Régimes d'écoulement en milieu poreux et limite de la loi de Darcy. La Houille Blanche 2, 141–148. http://dx.doi.org/10.1051/lhb/1967009.

Chen, Z., Lyons, S.L., Qin, G., 2001. Derivation of the Forchheimer law via homogenization. Transp. Porous Media 44 (2), 325–335. http://dx.doi.org/10.1023/A:1010749114251.

Chevalier, T., Chevalier, C., Clain, X., Dupla, J.C., Canou, J., Rodts, S., Coussot, P., 2013. Darcy's law for yield stress fluid flowing through a porous medium. J. Non Newton. Fluid Mech. 195, 57–66.

Chevalier, T., Rodts, S., Chateau, X., Chevalier, C., Coussot, P., 2014. Breaking of non-Newtonian character in flows through a porous medium. Phys. Rev. E 89, 023002.

Christopher, R.H., Middleman, S., 1965. Power-law flow through a packed tube. Ind. Eng. Chem. Fundam. 4 (4), 422–426.

Ciriello, V., Longo, S., Chiapponi, L., Di Federico, V., 2016. Porous gravity currents: a survey to determine the joint influence of fluid rheology and variations of medium properties. Adv. Water Res. 92, 105–115.

Comba, S., Dalmazzo, D., Santagata, E., Sethi, R., 2011. Rheological characterization of xanthan suspensions of nanoscale iron for injection in porous media. J. Hazard. Mater. 185, 598–605.

Cvetkovic, V.D., 1986. A continuum approach to high velocity flow in a porous medium. Transp. Porous Media 1 (1), 63–97. http://dx.doi.org/10.1007/BF01036526.

Darcy, H.J., 1856. Les Fontaines Publiques de la Vue de Dijon. Libraire de Corps Imperiaux des Ponts et Chausees et des Mines. Paris, pp. 590–594.

Di Federico, V., Longo, S., Chiapponi, L., Archetti, R., Ciriello, V., 2014. Radial gravity currents in vertically graded porous media: theory and experiments for Newtonian and power-law fluids. Adv. Water Res. 70, 65–76.

Dullien, A.L., Azzam, M.I.S., 1973. Flow rate-pressure gradient measurement in periodically nonuniform capillary tube. AIChE J. 19, 222–229. http://dx.doi.org/10.1002/aic.690190204.

Dybbs, A., Edwards, R.V., 1984. A new look at porous media fluid mechanics – Darcy to turbulent. In: Bear, J., Corapcioglu, M.Y. (Eds.). NATO ASI Series, Series E,, Fundamentals of Transport Phenomena in Porous Media. Martinus Nijhoff Publishers The Hague.

Dukhan, N., Patel, K., 2011. Effect of sample's length on flow properties of open-cell metal foam and pressure-drop correlations. J. Porous Mater. 18 (6), 655–665.

Dukhan, N., Bağcı, Ö., Özdemir, M., 2014. Experimental flow in various porous media and reconciliation of Forchheimer and Ergun relations. Exp. Therm. Fluid Sci. 57, 425–433. http://dx.doi.org/10.1016/j.expthermflusci.2014.06.011.

Ergun, S., 1952. Fluid flow through packed columns. Chem. Eng. Prog. 48, 89–94.

Fadili, A., Tardy, P., Pearson, J., 2002. A 3D filtration law for power-law fluids in heterogeneous porous media. J. Non Newton. Fluid Mech. 106, 121–146.

Fang, J., Zhu, T., Sheng, J., Jiang, Z., Ma, Y., 2015. Thickness dependent effective viscosity of a polymer solution near an interface probed by a quartz crystal microbalance with dissipation method. Sci. Rep. 5. http://dx.doi.org/10.1038/srep08491, Article number: 8491.

Forchheimer, P., 1901. Wasserberwegng durch Boden. Forschtlft ver. D. Ing. 45 (50), 1782–1788.

Fourar, M., Radilla, G., Lenormand, R., Moyne, C., 2004. On the non-linear behavior of a laminar single-phase flow through two and three-dimensional porous media. Adv. Water Resour. 27, 669–677.

Garcia-Ochoa, F., Santosa, V.E., Casasb, J.A., Gómez, E., 2000. Xanthan gum: production, recovery, and properties. Biotechnol. Adv. 18, 549–579.

Giorgi, T., 1997. Derivation of the Forchheimer law via matched asymptotic expansions. Transp. Porous Media 29 (2), 191–206. http://dx.doi.org/10.1023/A:1006533931383.

González, J.M., Müller, A.J., Torres, M.F., Sáez, A.E., 2005. The role of shear and elongation in the flow of solutions of semi-flexible polymers through porous media. Rheol. Acta 44, 396–405. http://dx.doi.org/10.1007/s00397-004-0421-4.

Fayed, H.E., Sheikh, N.A., Iliev, O., 2016. On Laminar flow of non-Newtonian fluids in porous media. Transp. Porous Media 111, 253–264.

Geertsma, M., 1974. Estimating the coefficient of inertial resistance fluid flow through porous media. SPE J. 14 (5), 445–450. http://dx.doi.org/10.2118/4706-PA.

Hirasaki, G.J., Pope, G.A., 1974. Analysis of factors influencing mobility and adsorption in the flow of polymer solution through porous media. SPE J. 14 (4), 337–347.

Hubbert, M.K., 1956. Darcy law and the field equations of the flow of underground fluids. Trans. Am. Inst. Min. Metall. Eng. 207, 222–239.

Hwang, J.J., Hwang, G.J., Yeh, R.H., Chao, C.H., 2002. Measurement of interstitial convective heat transfer and frictional drag for flow across metal foams. J. Heat Transf. 124, 120–129.

Kaviany, M., 1995. Principles of Heat Transfer in Porous Media. Springer, New York, p. 3. Ch.2.

Kececioglu, I., Jiang, Y., 1994. Flow through porous media of packed spheres saturated with water. J. Fluids Eng. 116, 164–170.

Klump, M., Inayat, A., Schwerdtfeger, J., Koner, C., Singer, R.F., Freund, H., Scheieger, W., 2014. Periodic open cell structures with ideal cubic cell geometry: effect of porosity and cell orientation on pressure drop. Chem. Eng. J. 242, 364–378.

Lage, J.L., Antohe, B.V., 2000. Darcy's Experiments and the deviation to nonlinear flow regime. J. Fluids Eng. 122, 619–625.

Liu, J.F., Wo, W.T., Chiu, W.C., Hsieh, W.H., 2006. Measurement and correlation of friction characteristic of flow through foam matrixes. Exp. Therm. Fluid Sci. 30, 329–336.

Longo, S., Ciriello, V., Chiapponi, L., Di Federico, V., 2015a. Combined effect of rheology and confining boundaries on spreading of porous gravity currents. Adv. Water Resour. 79, 140–152.

Longo, S., Di Federico, V., Chiapponi, L., 2015b. A dipole solution for power-law gravity currents in porous formations. J. Fluid Mech. 778, 534–551.

Longo, S., Di Federico, V., Chiapponi, L., Archetti, R., 2013. Experimental verification of power-law of non-Newtonian axisymmetric porous gravity currents. J. Fluid Mech. 731, R2.

López, X., Valvatne, P.H., Blunt, M.J., 2003. Predictive network modeling of single-phase non-Newtonian flow in porous media. J. Colloid Interface Sci. 264 (1), 256–265. http://dx.doi.org/10.1016/s0021-9797(03)00310-2.

López, X., 2004. Pore-Scale Modelling of Non-Newtonian Flow, Ph.D. thesis, Department of Earth Science & Engineering Petroleum Engineering & Rock Mechanics Group, Imperial College, London.

MacDonald, I.F., El-Sayed, M.S., Mow, K., Dullien, F.A.L., 1979. Flow through porous media, the Ergun equation revisited. Ind. Eng. Chem. Fundam. 18 (3), 199–208. http://dx.doi.org/10.1021/i160071a001.

Machac, I., Cakl, J., Comiti, J., Sabiri, N.E., 1998. Flow of non-Newtonian fluids through fixed beds of particles: comparison of two models. Chem. Eng. Process. 37, 169–176.

Meurant, G., 1981. Enhanced oil recovery. In: Proceedings of the Third European Symposium on Enhanced Oil Recovery. Bournemouth, U.K.. Elsevier Science September 21-23.

Mongruel, A., Cloitre, M., 2003. Axisymmetric orifice flow for measuring the elongational viscosity of semi-rigid polymer solutions. J. Non Newton. Fluid Mech. 110, 27–43.

Müller, A.J., Sáez, A.E., 1999. The rheology of polymer solutions in porous media. In: Nguyen, T.Q., Kausch, H.H. (Eds.), Flexible Polymer Chain Dynamics in Elongational Flow: Theory and Experiment. Springer, Heidelberg, pp. 335–393.

Nguyen, T.Q., Kausch, H.H., 1999. Flexible Polymer Chains in Elongational Flow: Theory and Experiment. Springer, Berlin.

Palaniraj, A., Jayaraman, V., 2011. Production, recovery and applications of xanthan gum by Xanthomonas campestris. J. Food Eng. 106, 1–12.

Pang, Z., Liu, H., 2013. The study on permeability reduction during steam injection in unconsolidated porous media. J. Pet. Sci. Eng. 106, 77–84. http://dx.doi.org/10.1016/j.petrol.2013.04.022.

Perrin, C.L., Tardy, P.M.J., Sorbie, K.S., Crawshaw, J.C., 2006. Experimental and modeling study of Newtonian and non-Newtonian fluid flow in pore network micromodels. J. Colloid Interface Sci. 295 (2), 542–550. http://dx.doi.org/10.1016/j.jcis.2005.09.012.

Pauchard, L., Varela López, F., Rosen, M., Allain, C., Perrot, P., Rabaud, M., 1999. On the effects of non-Newtonian fluids above the ribbing instability. In: Proceedings of the European Coating Symposium on Advances in Coating and Drying of Thin Films, pp. 183–188.

Rao, P.T., Chhabra, R.P., 1993. Viscous non-Newtonian flow in packed beads: effects of column walls and particle size distribution. Powder Technol. 77, 171–176.

Rasoloarijaona, M., Auriault, J.L., 1994. Nonlinear seepage flow through a rigid porous medium. Eur. J. Mech. B Fluids 13 (2), 177–195.

Radilla, G., Nowamooz, A., Fourar, M., 2013. Modeling non-Darcian single- and two-phase flow in transparent replicas of rough-walled rock fractures. Transp. Porous Media 98, 401–426. http://dx.doi.org/10.1007/s11242-013-0150-1.

Rodríguez, S., Romero, C., Sargenti, M.L., Müller, A.J., Sáez, A.E., Odell, J.A., 1993. Flow of polymer solutions through porous media. J. Non Newton. Fluid Mech. 49, 63–85.

Rodríguez de Castro, A, Omari, A., Ahmadi-Sénichault, A., Bruneau, D., 2014. Toward a new method of porosimetry: principles and experiments. Transp. Porous Media 101 (3), 349–364. http://dx.doi.org/10.1007/s11242-013-0248-5.

Rodríguez de Castro, A, Omari, A., Ahmadi-Sénichault, A., Savin, S., Madariaga, L.-F., 2016a. Characterizing porous media with the yield stress fluids porosimetry method. Transp. Porous Media 114, 213–233. http://dx.doi.org/10.1007/s11242-016-0734-7.

Rodríguez de Castro, A., Oostrom, M., Shokri, N., 2016b. Effects of shear-thinning fluids on residual oil formation in microfluidic pore networks. J. Colloid Interface Sci. 472, 34–43. http://dx.doi.org/10.1016/j.jcis.2016.03.027.

Rodríguez de Castro, A, Radilla, G., 2016. Non-Darcian flow experiments of shear-thinning fluids through rough-walled rock fractures. Water Resour. Res. 52. http://dx.doi.org/10.1002/2016WR019406.

Ruth, D., Ma, H., 1992. On the derivation the Forchheimer equation by means of the averaging theorem. Transp. Porous Media 7, 255–264.

Sabiri, N.-E., Comiti, J., 1995. Pressure drop in non-Newtonian purely viscous fluid flow through porous media. Chem. Eng. Sci. 50, 1193–1201.

Saggin, R., Coupland, J.N., 2004. Rheology of xanthan/sucrose mixtures at ultrasonic frequencies. J. Food Eng. 65, 49–53.

Scheidegger, A.E., 1960. The Physics of Flow Through Porous Media. Macmillan, New York.

Schneebeli, G., 1955. Expériences sur la limite de validité de la loi de Darcy et l'apparition de la turbulence dans un écoulement de filtration. La Houille Blanche 2, 141–149. http://dx.doi.org/10.1051/lhb/1955030.

Seright, R.S., Fan, T., Wavrik, K., de Carvalho Balaban, R., 2011. New insights into polymer rheology in porous media. SPE J. 16, 35–42. http://dx.doi.org/10.2118/129200-PA.

Shah, C.B., Yortsos, Y.C., 1995. Aspects of flow of power-law fluids in porous media. AIChE J. 41 (5), 1099–1112.

Shenoy, A.V., 1994. Non-Newtonian fluid heat transfer in porous media. Adv. Heat Transf. 24, 101–190.

Silva, J.A.K., Smith, M., Munakata-Marr, J., McCray, J.E., 2012. The effect of system variables on in situ sweep-efficiency improvements via viscosity modifications. J. Contam. Hydrol. 136, 117–130.

Smit, G.J.F., du Plessis, J.P., 1997. Pressure drop prediction of power law fluid through granular media. J. Non Newton. Fluid Mech. 72, 319–323.

Sochi, T., 2010. Non-Newtonian flow in porous media. Polymer 51, 5007–5023.

Song, Y.-Q., 2007. Novel NMR techniques for porous media research. Cem. Concr. Res. 37, 325–328.

Sorbie, K.S., Clifford, P.J., Jones, E.R.W., 1989. The rheology of pseudoplastic fluids in porous media using network modeling. J. Colloid Interface Sci. 130 (2), 508–534.

Tiu, C., Zhou, J.Z.Q., Nicolae, G., Fang, T.N., Chhabra, R.P., 1997. Flow of viscoelastic polymer solutions in mixed beds of particles. Can. J. Chem. Eng. 75, 843–850.

Tosco, T., Marchisio, D.L., Lince, F., Sethi, R., 2013. Extension of the Darcy–Forchheimer law for shear-thinning fluids and validation via pore-scale flow simulations. Transp. Porous Media 96, 1–20. http://dx.doi.org/10.1007/s11242-012-0070-5.

Wadhai, V.S., Dixit, A.N., 2011. Production of Xanthan gum by Xanthomonas campestris and comparative study of Xanthomonas campestris isolates for the selection of potential Xanthan producer. Indian Streams Res. J. 1, 1–4.

Wengeler, L., 2014. Coating and Drying Processes for Functional Films in Polymer Solar Cells – From Laboratory to Pilot Scale. KIT Scientific Publishing, Karlsruhe.

Woudberg, S., Du Plessis, J.P., Smit, G.J.F., 2006. Non-Newtonian purely viscous flow through isotropic granular porous media. Chem. Eng. Sci. 61, 4299–4308.

Xin, J., Zheng, X., Han, J., Shao, H., Kolditz, O., 2015. Remediation of trichloroethylene by xanthan gum-coated microscale zero valent iron (XG-mZVI) in groundwater: effects of geochemical constituents. Chem. Eng. J. 271, 164–172.

Zeng, Z., Grigg, R., 2006. A criterion for non-Darcy flow in porous media. Transp. Porous Media 63, 57–69. http://dx.doi.org/10.1007/s11242-005-2720-3.